J Mater Sci: Mater Electron (2017) 28:14839–14847
DOI 10.1007/s10854-017-7355-y

Preparation, characterization, and dielectric properties of $CaCu_3Ti_4O_{12}$-related $(Na_{1/3}Ca_{1/3}Y_{1/3})Cu_3Ti_4O_{12}$ ceramics using a simple sol–gel method

Jutapol Jumpatam[1] · Areeya Moontang[2] · Bundit Putasaeng[3] · Pinit Kidkhunthod[4] · Narong Chanlek[4] · Prasit Thongbai[2,5]

Received: 9 April 2017 / Accepted: 13 June 2017 / Published online: 16 June 2017

Abstract $(Na_{1/3}Ca_{1/3}Y_{1/3})Cu_3Ti_4O_{12}$ nanoparticles with sizes of about 100–200 nm are successfully prepared using simple sol–gel method. The main phase of $(Na_{1/3}Ca_{1/3}Y_{1/3})Cu_3Ti_4O_{12}$ is obtained in both powders and sintered ceramics. Microstructural analysis confirms the presence of Na, Ca, Y, Cu, Ti, and O and these elements are well dispersed in the microstructure. The average grain size of $(Na_{1/3}Ca_{1/3}Y_{1/3})Cu_3Ti_4O_{12}$ ceramics significantly increases with increasing sintering times. High dielectric permittivity and low loss tangent values of about 2.52×10^4 and 0.034 (at 1 kHz), respectively, are achieved. $(Na_{1/3}Ca_{1/3}Y_{1/3})Cu_3Ti_4O_{12}$ ceramics can exhibit non-Ohmic properties with a breakdown electric field and nonlinear coefficient of $\approx5.2\times10^3$ V/cm and 7.91, respectively. Investigation of the DC bias dependence of the electric responses confirms that the giant dielectric properties originate from the internal barrier layer capacitance effect. The presence of Cu^+, Cu^{3+}, and Ti^{3+} ions is confirmed and suggested to have an influence on conduction in semiconducting grains.

✉ Prasit Thongbai
pthongbai@kku.ac.th

1 Materials Science and Nanotechnology Program, Faculty of Science, Khon Kaen University, Khon Kaen 40002, Thailand

2 Integrated Nanotechnology Research Center (INRC), Department of Physics, Faculty of Science, Khon Kaen University, Khon Kaen 40002, Thailand

3 National Metal and Materials Technology Center, 114 Thailand Science Park, Paholyothin Rd. Klong 1, Klong Luang, Pathunthani 12120, Thailand

4 Synchrotron Light Research Institute (Public Organization), 111 University Avenue, Muang District, Nakhon Ratchasima 30000, Thailand

5 Nanotec–KKU Center of Excellence on Advanced Nanomaterials for Energy Production and Storage, Khon Kaen 40002, Thailand

1 Introduction

Over the past few years, the giant dielectric properties of a series of isostructural $CaCu_3Ti_4O_{12}$ (CCTO)-type perovskites have been widely investigated [1–21]. This is because CCTO and CCTO-related oxides exhibit very high dielectric permittivity (ε') values of 10^4 over a wide temperature range. Such high ε' values were found to be stable with temperature in the range of 100–400 K. These oxides were believed to be a promising material for capacitor applications. Furthermore, the physical characteristics explaining the giant dielectric response in polycrystalline CCTO ceramics is still unclear. Nevertheless, it is widely believed that the internal barrier layer capacitor (IBLC) effect based on Maxwell–Wagner polarization (or interfacial polarization) at the grain boundaries (GBs) is the primary cause of the giant dielectric response in CCTO and related oxides [22–25]. This IBLC model was confirmed by impedance spectroscopy and microprobe analyses [26, 27]. The microstructure consisted of *n*-type semiconducting grains and insulating GBs. However, the intrinsic effect cannot be ignored [28, 29]. In addition to the giant dielectric properties, CCTO and related ceramics can also exhibit non-Ohmic properties [14, 27].

Unfortunately, a high loss tangent ($\tan\delta > 0.05$ at 1 kHz) of CCTO and related ceramics is still unsuitable for capacitor applications [4, 6, 10, 12, 29]. Therefore, investigation to reduce the $\tan\delta$ of CCTO ceramics is still a challenge. Doping CCTO and related oxides with suitable ions is a generally used method to improve their dielectric properties. Interestingly, a reduction in $\tan\delta$ values to less than

0.05 was achieved by doping with ions such as La^{3+} [30], and Mg^{2+} [14].

Except for CCTO, the family of $ACu_3Ti_4O_{12}$ related-oxides (where A = Cd, $Y_{2/3}$, $La_{2/3}$, $Bi_{2/3}$, $Na_{1/2}La_{1/2}$, $Na_{1/2}Bi_{1/2}$, $Na_{1/2}Y_{1/2}$, $Na_{1/3}Ca_{1/3}Bi_{1/3}$, and $Na_{1/3}Ca_{1/3}Y_{1/3}$) can exhibit improved giant ε' and non-Ohmic properties [1, 2, 10, 13, 17, 20, 22, 31]. The giant dielectric response was widely ascribed to the IBLC effect. Another sub-family of $ACu_3Ti_4O_{12}$ materials, in which the A-site was randomly occupied by +1, +2 and +3 valence charged ions, each at a level about of ~33.3 at.%, was reported. Good dielectric properties of $[Na^+_{1/3}Ca^{2+}_{1/3}Ln^{3+}_{1/3}]Cu_3Ti_4O_{12}$, where Ln^{3+} can be Bi and Y, were reported [10, 13, 31]. For example, low tanδ (~0.038) and a high ε' values (~2.5×10^4) were obtained in $(Na_{1/3}Ca_{1/3}Bi_{1/3})Cu_3Ti_4O_{12}$ ceramics [10]. Additionally, several chemical solution routes and control of sintering conditions for synthesis of CCTO and related oxides have been widely used to significantly improve their dielectric properties [6, 17, 20, 32]. A shorter reaction time and lower temperature were sufficient for their synthesis due to the homogeneity of the starting materials at an atomic scale. Improved dielectric properties of CCTO ceramics prepared using a sol–gel method were studied by Sun et al. [33]. They reported a high ε′ value of about 1.8×10^4 with a low tanδ ~0.03 at 1 kHz and RT. Unfortunately, $[Na^+_{1/3}Ca^{2+}_{1/3}Ln^{3+}_{1/3}]Cu_3Ti_4O_{12}$ ceramics prepared via a chemical route have never been reported.

In the work, $(Na_{1/3}Ca_{1/3}Y_{1/3})Cu_3Ti_4O_{12}$ (NCYCTO) ceramics were prepared using a simple sol–gel method. Their phase formation, microstructure, dielectric response, and electrical properties were systematically investigated. It was found that the highest ε' value of this ceramic system was 2.5×10^4 and a low tanδ values of ~0.04 were measured at 1 kHz. The origin of the giant dielectric response and nonlinear electrical properties are discussed.

2 Experimental details

NCYCTO ceramics were prepared using a simple sol–gel method (SSG). First, a stoichiometric amount of each starting material, i.e., $NaCH_3COO$, $(CH_3CO_2)_3Y{\cdot}H_2O$, $Ca(C_2H_3CO_2)_2{\cdot}H_2O$, and $Cu(CH_3COO)_2{\cdot}H_2O$ were dissolved in an aqueous solution of citric acid (5 wt%) and ethylene glycol with constant stirring at RT. Second, $C_{16}H_{28}O_6Ti$ was dissolved in the above solution under continued stirring. After that, ethanol was added drop wise into the solution at 150 °C until it formed a viscous gel. Then, the gel was dried in air at 350 °C for 40 min. Samples of the resulting porous and dried precursor were ground and calcined at 800, 850 and 900 °C for 6 h (referred to as the C800, C850, and C900 powders, respectively). All calcined powders were carefully re-ground and pressed into pellets, ~1.0 mm in thickness and 9.5 mm in diameter, by uniaxial compression at about 200 MPa. Finally, these pellets were sintered in air at 1080 °C for 4, 8 and 16 h.

The crystal structure and phase composition of the calcined powders and sintered ceramics were measured using an X-ray diffraction (XRD) technique (PANalytical, EMPYREAN). Scanning electron microscopy (SEM) (SEC, SNE4500M) was used to reveal the microstructure of the sintered ceramics. Before the surface morphology measurements, the as-sintered ceramics were carefully polished and thermally etched at 1040 °C for 20 min. The distribution of elements, i.e., Na, Ca, Y, Cu, Ti and O, in the sintered NCYCTO ceramic was investigated using field-emission scanning electron microscopy (FE-SEM) with energy-dispersive X-ray analysis (EDX) (HITACHI SU5030, Japan). X-ray Absorption Near Edge Structure (XANES) spectra were measured at the SUT-NANOTEC-SLRI XAS beamline (BL5.2), the Synchrotron Light Research Institute (SLRI), Nakhon Ratchasima, Thailand. Details of this characterization technique and analysis are given elsewhere [14]. The normalized XANES data were corrected and analyzed after background subtraction in the pre-edge and post-edge region using ATHENA software included in an IFEFFIT package [34]. The sintered ceramics were also characterized using X-ray photoelectron spectroscopy (XPS), (PHI5000 VersaProbe II, ULVAC-PHI, Japan) at the SUT-NANOTEC-SLRI Joint Research Facility, Synchrotron Light Research Institute (SLRI), Thailand. The XPS spectra were fitted with PHI MultiPak XPS software using Gaussian–Lorentzian lines.

For dielectric measurements, Au electrodes were made by sputtering Au on each pellet face at a current of 30 mA for 8 min using a Polaron SC500 sputter coating unit. The dielectric properties were measured using a KEYSIGHT E4990A Impedance Analyzer using a capacitance-dissipation factor mode. An oscillation voltage of 500 mV was used. The measurements were done over the frequency and temperature ranges of 10^2–10^7 Hz and −70 to 200 °C, respectively. Each measured temperature was kept constant with an accuracy of less than ±0.1 °C. The dielectric properties under DC bias voltage were measured in the range of 0–40 V at RT. Nonlinear current density–electric field strength (J–E) characteristics were investigated using a high voltage measurement unit (Keithley Model 247) at RT. The breakdown electric field (E_b) and nonlinear coefficient (α) were obtained at $J = 1$ mA cm^{-2} and calculated in the range of at $J = 1$–10 mA cm^{-2}, respectively.

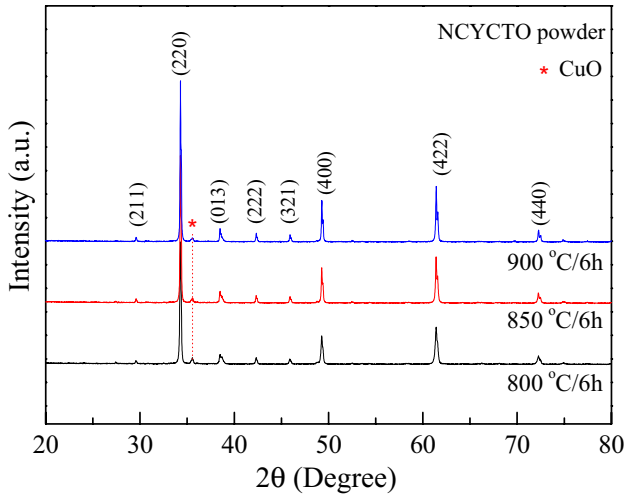

Fig. 1 XRD patterns of C800, C850, and C900 powders

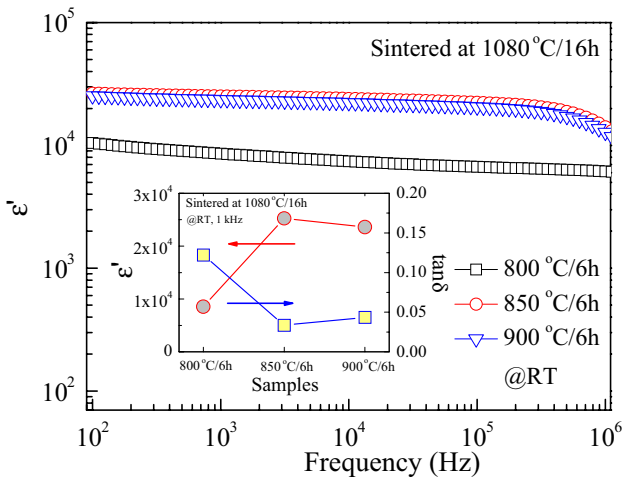

Fig. 2 Frequency dependence of ε′ at RT of NCYCTO ceramics sintered at 1080 °C for 16 h fabricated from the C800, C850, and C900 powders; *inset* shows the summarized values ε′ and tanδ at 1 kHz and RT

3 Results and discussion

The XRD patterns of NCYCTO powders prepared using the SSG method and calcined at different temperatures are illustrated in the Fig. 1. A primary phase of NCYCTO is detected in the XRD patterns of all powders. These XRD patterns confirm the formation of a CCTO-like phase (JCPDS card no. 75-2188). All the diffraction peaks are well indexed based on the body-centered cubic structure within space group $Im\bar{3}$. A small amount of a CuO impurity phase is observed in all powders. The lattice parameters of the C800, C850, and C900 powders were 7.389, 7.388, and 7.387 Å, respectively. These values are between the corresponding values of CCTO (7.391 Å) [1] and $Na_{1/2}Y_{1/2}Cu_3Ti_4O_{12}$ (7.381–7.387 Å) [2, 13, 31]. This is due to the difference in the ionic radii of the A-sites. A Ca^{2+} ion (0.99 Å) is larger than that of the average Na^{+} (0.95 Å) and Y^{3+} (0.93 Å) ions. Na^{+}, Ca^{2+} and Y^{3+} ions randomly occupied the A-site of the $ACu_3Ti_4O_{12}$ structure.

Figure 2 shows the dielectric properties of the NCYCTO ceramics sintered at 1080 °C for 16 h using powders that were calcined at different temperatures. The inset of Fig. 2 shows ε′ and tanδ values measured at 1 kHz and RT for the sintered ceramics. The ε′ (tanδ) values of the sintered NCYCTO ceramics using the C800, C850, and C900 powders are about 8.6×10^3 (0.122), 2.5×10^4 (0.034) and 2.4×10^4 (0.046), respectively. These interesting dielectric properties are achieved in the sintered ceramics using C850 and C900 powders. The C850 powder was further used to prepare ceramic samples sintered at 1080 °C for 4, 8 and 16 h (referred to as the NCY_4 h, NCY_8 h and NCY_16 h ceramics, respectively) since its bulk ceramic has the best dielectric properties. It is notable that the dielectric properties of the NCYCTO ceramic prepared using the SSG method is better that those of NCYCTO ceramics prepared by a conventional solid state reaction method [13, 31]. The influences of sintering time on the dielectric and electrical properties of NCYCTO ceramics were studied as follows.

Figure 3 shows the Rietveld refinement profile fit of the C850 powder and all sintered ceramics, confirming the presence of a primary phase of NCYCTO, which has a CCTO-like structure [1, 2]. According to the Rietveld refinement, lattice parameters of the NCY_4 h, NCY_8 h, and NCY_16 h ceramics are 7.387, 7.382 and 7.381 Å, respectively. These values are very close to that obtained in NCYCTO prepared using a solid state reaction method (for 7.387 Å) [31].

Figure 4a shows a TEM image of NCYCTO particles calcined at 850 °C for 6 h. The particle sizes are about 100–300 nm. The surface morphologies of the NCYCTO ceramics sintered at 1080 °C for different sintering times are shown in Fig. 4b–d. The average grain sizes of the NCY_4 h, NCY_8 h and NCY_16 h ceramics are estimated to be 6.7 ± 2.9, 7.1 ± 3.6 and 14.5 ± 6.9 μm, respectively. For a CCTO polycrystalline ceramic, grain growth is usually described by a liquid phase sintering mechanism [7]. The eutectic temperature of $CuO–TiO_2$ is about ≈950 °C [6]. Therefore, this liquid phase can appear during sintering process, giving rise to an increased grain growth rate. This mechanism can be responsible for the observed enlargement of the mean grain size of the NCYCTO ceramics. Segregation of some particles with irregular shape is observed along the GBs, especially for the NCY_4 h ceramic.

Figure 5a shows the EDS spectrum of the NCY_16 h ceramic measured in a selected area (its inset), confirming the

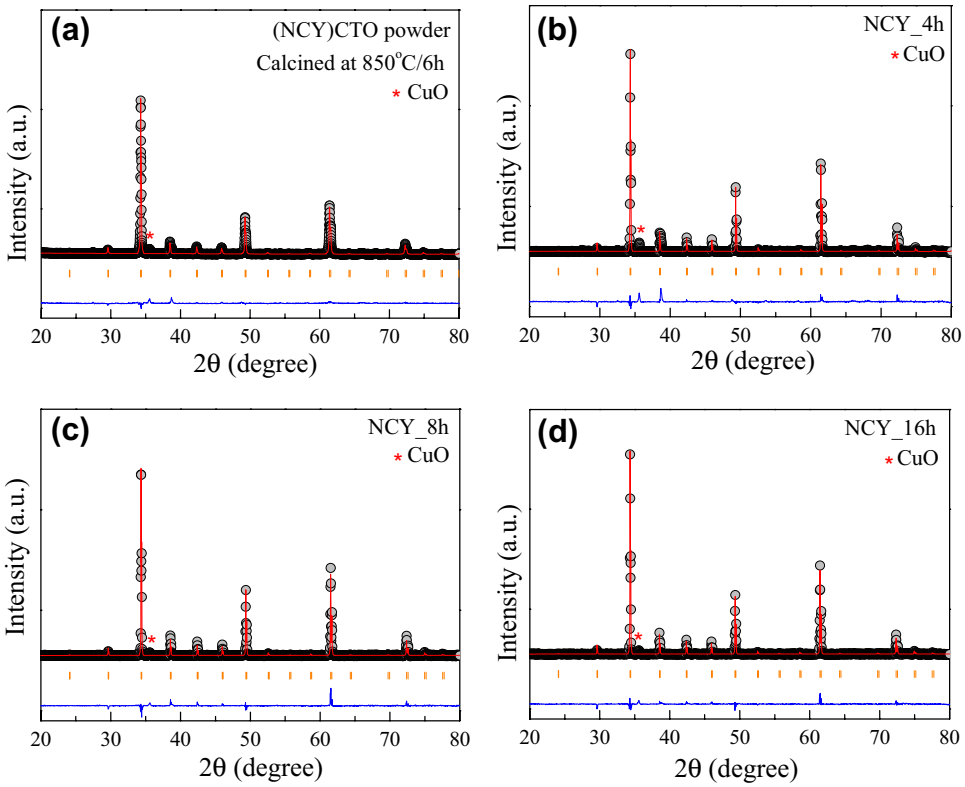

Fig. 3 Profile fits for Rietveld refinements of **a** C850 powder, **b** NCY_4 h, **c** NCY_8 h, and **d** NCY_16 h samples

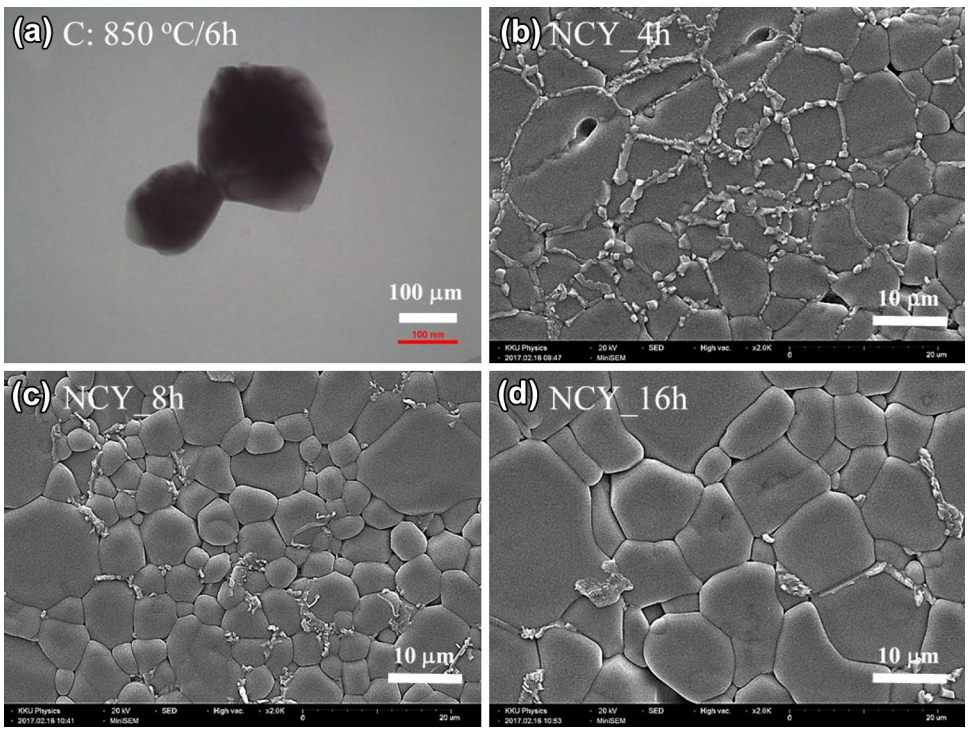

Fig. 4 **a** TEM image of C850 powder. **b**–**d** SEM images of polished surfaces of NCY_4 h, NCY_8 h, NCY_16 h samples, respectively

existence of all ions of interest in NCYCTO. SEM mapping images of Na, Ca, Y, Cu, Ti and O of the NCY_16 h ceramic are shown in Fig. 5b, revealing a homogeneous dispersion of each element in the microstructure. As illustrated in the inset of Fig. 5a, slight segregation of a CuO-rich phase is observed. This confirms that the particles with irregular shapes

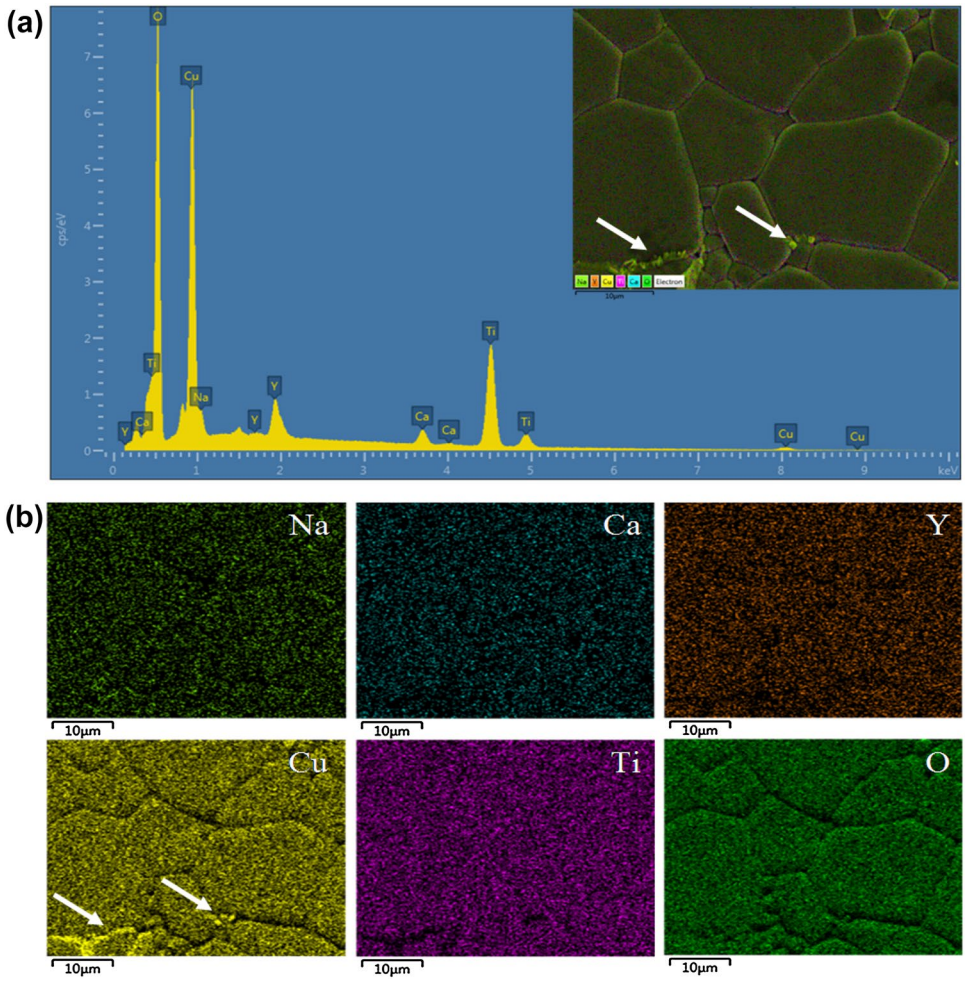

Fig. 5 **a** EDS spectra of the NCY_16 h sample; *inset* shows the selected area for SEM mapping. **b** Elemental mapping of the NCY_16 h sample, i.e., Na, Ca, Y, Cu, Ti, and O

observed in the NCYCTO ceramics are from the CuO-rich phase, corresponding to the XRD result.

The frequency dependence of the dielectric properties at RT of NCYCTO ceramics sintered at 1080 °C for different sintering times is shown in Fig. 6. In the range of 10^2–10^5 Hz, the ε′ values all the ceramic samples are independent of frequency. The ε′ values at RT and 1 kHz of the NCY_4 h, NCY_8 h and NCY_16 h ceramics are about 9.2×10^3, 1.3×10^4 and 2.5×10^4, respectively. Here, it is observed that ε′ increased with increasing average grain size. It is notable that these values are larger than those obtained in NCYCTO ceramics prepared using a solid state reaction method [13, 31]. The enhanced dielectric response can usually be associated with a change in microstructure, according to the IBLC model. The effective dielectric constant, ε'_{eff}, can be expressed as [35]:

$$\varepsilon'_{eff} = \frac{\varepsilon_{gb} d_g}{t_{gb}} \quad (1)$$

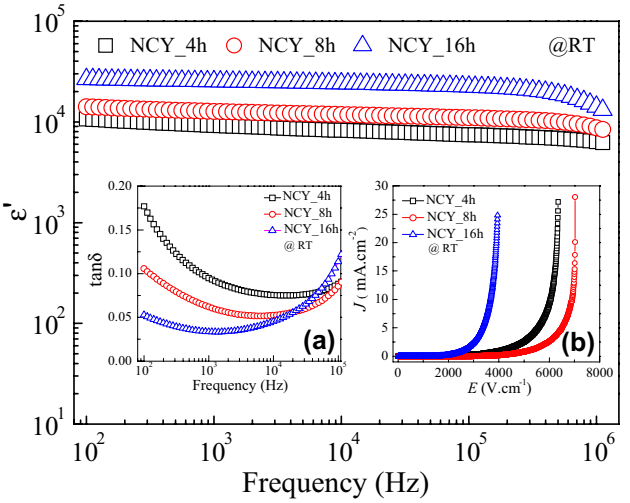

Fig. 6 ε′ at RT as a function of frequency for NCY_4 h, NCY_8 h and NCY_16 h samples. *Inset* (*a*) shows the tanδ values as a function of frequency at RT. *Inset* (*b*) shows nonlinear J–E characteristics at RT of all samples

where ε_{gb},d_g, and t_{gb} are the dielectric constant of the GB, the average grain size, and the GB thickness, respectively.

As shown in inset (a) of Fig. 6, tanδ in a low frequency range of all ceramics is greatly increased with decreasing frequency. This behavior may have been caused by either DC conductivity or related interfacial polarization of the heterogeneous microstructure [35]. At RT and 1 kHz, the tanδ values of the NCY_4 h, NCY_8 h and NCY_16 h samples are 0.095, 0.062 and 0.034, respectively. ε' increases with sintering time, while tanδ is reduced. High ε' with good frequency stability and low tanδ is successfully achieved in the NCY_16 h sample. This indicates that the NCY_16 h sample may have potential use for capacitor applications.

As illustrated in inset (b) of Fig. 6, all of the NCYCTO ceramics prepared using the SSG method exhibit nonlinear *J–E* characteristics. The α values of the NCY_4 h, NCY_8 h, and NCY_16 h ceramics at RT are, respectively, 5.85, 7.91, and 6.60, while the E_b values are 4.1×10^3, 5.2×10^3, and 2.6×10^3 V/cm, respectively. It is now widely accepted the nonlinear properties of CCTO and related compounds are likely caused by the formation of Schottky barriers at the GBs sandwiched by semiconducting grains [7, 14, 27].

As shown in Fig. 7a, the *Z** plots in the temperature range of 150 to 200 °C are well fitted by the following modified equation corresponding to an equivalent circuit as demonstrated in the inset (2) of Fig. 7(a) [22]:

$$Z^* = R_g + \frac{R_{gb}}{1 + \left(i\omega R_{gb} C_{gb}\right)^{\alpha}} \tag{2}$$

where α is a constant value ($0 < \alpha \leq 1$), C_g (R_g) and C_{gb} (R_{gb}) are the capacitance (resistance) of grains and GBs, respectively. The C_g is not accessible and the respective capacitor can simply be omitted from the circuit. This result confirms

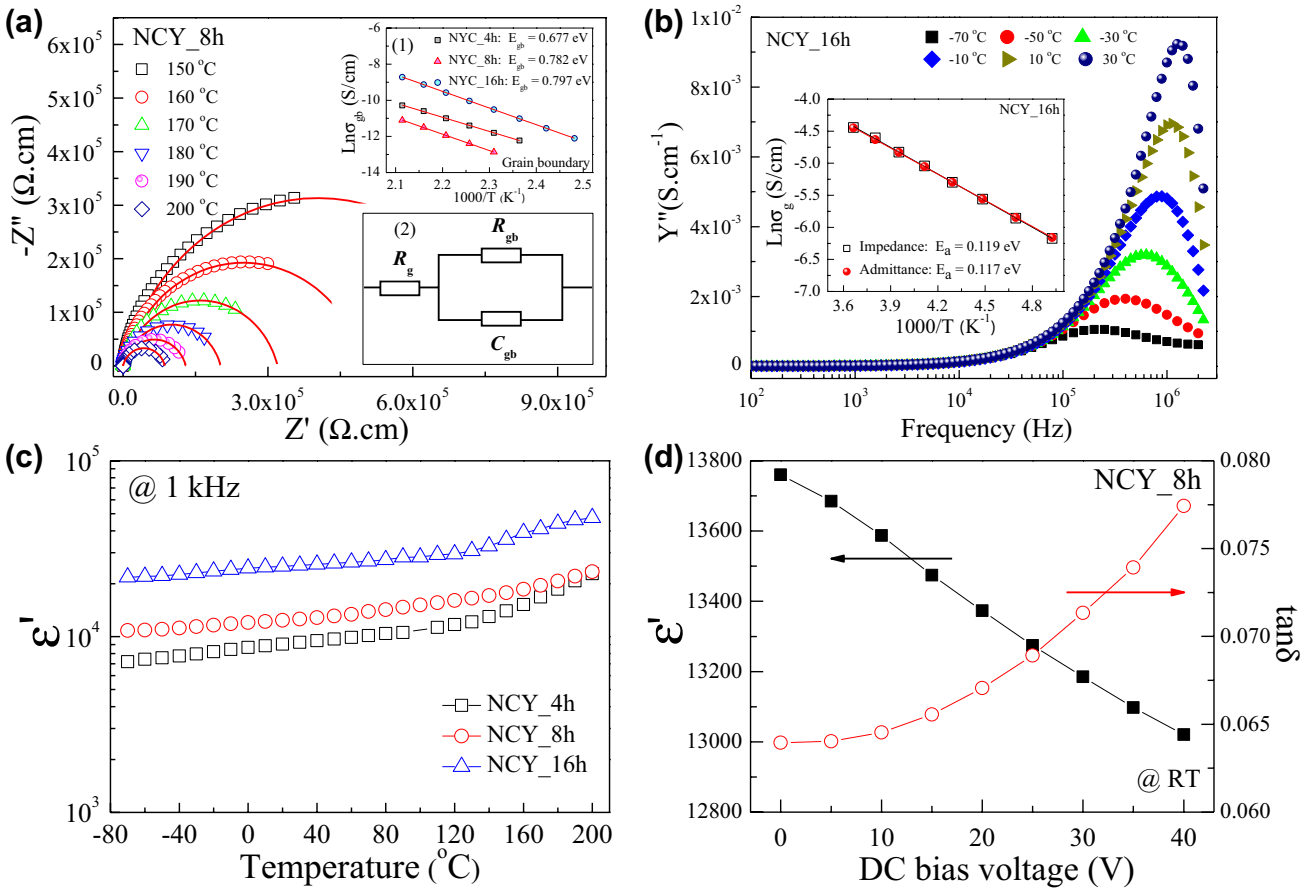

Fig. 7 **a** Z* plots for NCY_8 h sample at different temperatures (150–200 °C); the *red solid curves* are the fitted data using Eq. (2). *Inset* (*1*) of (**a**) shows Arrhenius plots of σ_{gb}; the *red solid lines* are the fitted data using Eq. (4). *Inset* (*2*) of (**a**) shows an equivalent circuit corresponding to Eq. (2). **b** Frequency dependence of Y″ at different temperatures for the NCY_16 h sample; *inset* shows Arrhenius plots for the temperature dependence of σ_g values obtained from impedance and admittance spectroscopy analyses. **c** Temperature dependence of ε′ at 1 kHz for NCYCTO ceramics. **d** ε′ and tanδ values at 1 kHz and RT for the NCY_8 h sample under DC bias voltages. (Color figure online)

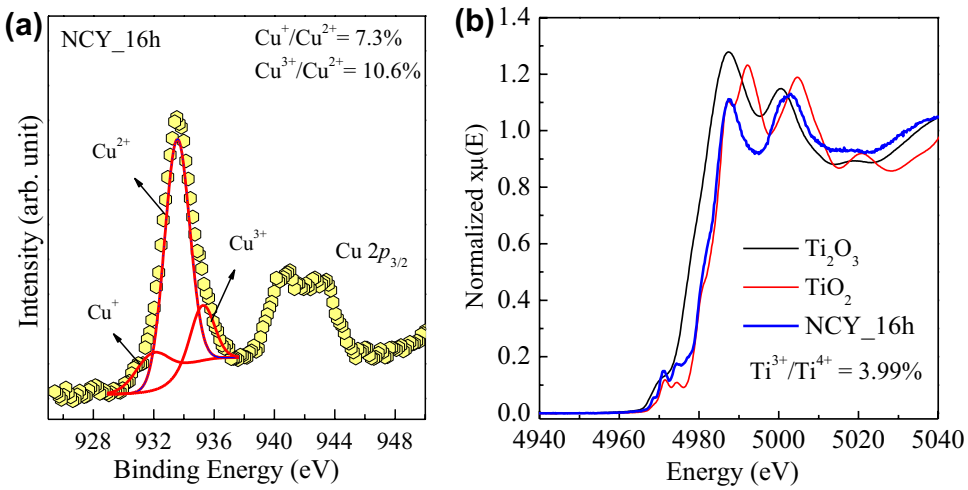

Fig. 8 **a** XPS spectrum of Cu *2p* region for the NCY_16 h sample. **b** Normalized XANES spectra for Ti *K*-edge of the NCY_16 h sample

that the microstructure of NCYCTO ceramics is electrically heterogeneous. In the inset (1) of Fig. 7a, the temperature dependencies of GB conductivity (σ_{gb}) follows the Arrhenius law:

$$\sigma_{gb} = \sigma_0 \exp\left(\frac{-E_{gb}}{k_B T}\right) \quad (3)$$

where σ_0 is a constant value, E_{gb} is the conduction activation energies at the GB, k_B is the Boltzmann constant and T is the absolute. The E_{gb} values of the NCY_4 h, NCY_8 h and NCY_16 h ceramics were calculated from the slopes of fitted data and found to be 0.677, 0.782, and 0.797 eV, respectively. E_{gb} significantly increases with increasing sintering times. These values are higher than 0.514–0.703 eV for NCYCTO ceramics prepared using a solid state reaction method [13, 31].

R_g values in a low temperature range can easily be calculated from the admittance spectroscopy analysis. As shown in Fig. 7b, Y″−peaks of the NCY_16 h ceramic appear in a low temperature range. Accordingly, R_g can be calculated from the relation, $R_g = 1/(2Y''_{max})$, where Y''_{max} is the maximum value at the peak of the imaginary part of complex admittance (Y*) [36]. As shown in the inset of Fig. 7b, the temperature dependence of the grain conductivity follows the Arrhenius law:

$$\sigma_g = \sigma_0 \exp\left(\frac{-E_g}{k_B T}\right) \quad (4)$$

where E_g is the conduction activation energies inside the grains. The experimental data obtained from the impedance and admittance spectroscopy analyses are well fitted using Eq. (4). Accordingly, the E_g values obtained from these analyses are 0.119 and 0.117 eV, respectively.

The temperature dependence of ε' at 1 kHz of NCYCTO ceramics is demonstrated in Fig. 7c. ε' slightly increases from −70 to 120 °C and then strongly increases at temperatures higher than 120 °C. This may have been caused by effect of DC conductivity, which is a one of factors corresponded to AC high tanδ values [4, 35]. Figure 7d shows the effects of DC bias voltage on the dielectric properties, i.e., ε' and tanδ values of the NCY_8h ceramic at RT. ε' decreases with increasing applied DC bias voltage, while tanδ greatly increases. This result may be associated with variation in the Schottky barrier height at the GBs as a result of applied DC bias [26]. With increasing DC bias voltage, the amount of accumulated charges is decreased because some charges can cross the insulating GBs. Consequently, the intensity of interfacial polarization at the GBs is reduced, giving rise to a decreased dielectric response [31]. Simultaneously, the DC conductivity increases due to the long range movement of free charges. A high loss tanδ associated with the reduction in ε' value is obtained under an increased DC bias voltage.

To explain the electrical conductivity of *n*-type semiconducting grains in the NCYCTO ceramic, the reactions of polyvalent cations ($Cu^{2+} \rightarrow Cu^{+}$ and $Ti^{4+} \rightarrow Ti^{3+}$) were investigated using XPS and XANES techniques. For the CCTO and $A_{2/3}Cu_3Ti_4O_{12}$ related ceramics, the presence of Cu^{+} and Ti^{3+} ions can cause formation of *n*-type semiconducting grains [25, 28, 29]. Figure 8a shows the XPS spectrum of Cu *2p* of the NCY_16 h sample. Three peaks are extracted from the XPS spectrum of Cu *2p* using Gaussian–Lorentzian profile fitting. The highest peak, with a binging energy 933.51 eV, is ascribed to Cu^{2+} [28, 29]. The peaks at 931.43 and 935.26 eV indicate the presence of Cu^{+} and Cu^{3+}, respectively [28, 37]. The ratios of Cu^{+}/Cu^{2+} and Cu^{3+}/Cu^{2+} are found to be 7.3 and 10.6%, respectively. Thus, the presence of Cu^{+} and Cu^{3+} has an

effect on the electrical conductivity of grains. The presence of Cu^{3+} might be associated with the segregation of a Cu-rich phase along the GBs [37], as shown in Fig. 4d. According to the XPS results, Ti^{3+} is difficult to detect, which may have been due to its low concentration. The XANES spectrum was further used to confirm the presence of Ti^{3+} to clearly describe electrical conductivity in the grain interiors. Figure 8b illustrates XANES spectra of the NCY_16 h sample, as well as the standard samples, i.e., Ti_2O_3 (Ti^{3+}) and TiO_2 (Ti^{4+}). The edge energy of the NCY_16 h sample is observed to closely match the TiO_2 standard. The presence of a small amount of Ti^{3+} is confirmed. The maximum value of the first derivative in the edge region is used to calculate the Ti^{3+}/Ti^{4+} ratio, which is 3.99%. It is reasonably to infer that electron hopping between $Ti^{3+} \leftrightarrow Ti^{4+}$ lattice sites may have also influenced the electrical conductivity of grains. The nature of electrical conductivity in grains is still complex. Nevertheless, it is reasonable to conclude that Cu^{+}, Cu^{3+} and Ti^{3+} ions have an effect on this property.

4 Conclusions

NCYCTO nanoparticles were successfully synthesized using a simple sol–gel method. Dense microstructure of sintered ceramics was obtained by employing NCYCTO nanoparticles. Na, Ca, Y, Cu, Ti, and O were well dispersed in the microstructure, indicating the formation of single phase. A high dielectric permittivity of 2.52×10^4 and low loss tangent of about 0.034 (at 1 kHz) were accomplished by optimization of preparation parameters. Good nonlinear *J*–*E* properties with $E_b = 5160$ V/cm and $\alpha = 7.91$ were also achieved. Through investigation of the DC bias dependence of the dielectric properties and using impedance spectroscopy, the giant dielectric response was attributed to the IBLC effect. It is suggested that the semiconducting grains of NCYCTO ceramics were induced by the presence of Cu^{+}, Cu^{3+}, and Ti^{3+} ions.

Acknowledgements This work was financially supported by the Thailand Research Fund (TRF) and Khon Kaen University, Thailand (Contract No. RSA5880012). It was partially supported by the Nanotechnology Center (NANOTEC), NSTDA, Ministry of Science and Technology, Thailand, through its program of Center of Excellence. The authors would like to thank the Synchrotron Light Research Institute (BL5.2) (Public Organization), Nakhon Ratchasima, Thailand for XANES measurements and the SUTNANOTEC-SLRI Joint Research Facility for XPS facility. J. Jumpatam would like to thank the Thailand Research Fund under The Royal Golden Jubilee Ph.D. Program (Grant Number PHD/0079/2557) for his Ph.D. scholarship.

References

1. M.A. Subramanian, D. Li, N. Duan, B.A. Reisner, A.W. Sleight, J. Solid State Chem. **151**, 323–325 (2000)
2. M.A. Subramanian, A.W. Sleight, Solid State Sci. **4**, 347–351 (2002)
3. L. Liu, H. Fan, L. Wang, X. Chen, P. Fang, Philos. Mag. **88**, 537–545 (2008)
4. Q. Zheng, H. Fan, C. Long, J. Alloys Compd. **511**, 90–94 (2012)
5. R. Löhnert, H. Bartsch, R. Schmidt, B. Capraro, J. Töpfer, A. Feteira, J. Am. Ceram. Soc. **98**, 141–147 (2015)
6. L. Singh, B.C. Sin, I.W. Kim, K.D. Mandal, H. Chung, Y. Lee, J. Varela, J. Am. Ceram. Soc. **99**, 27–34 (2016)
7. J. Jumpatam, B. Putasaeng, T. Yamwong, P. Thongbai, S. Maensiri, Mater. Res. Bull. **77**, 178–184 (2016)
8. A. Nautiyal, C. Autret, C. Honstettre, S. De Almeida-Didry, M. El Amrani, S. Roger, B. Negulescu, A. Ruyter, J. Eur. Ceram. Soc. **36**, 1391–1398 (2016)
9. R. Löhnert, B. Capraro, S. Barth, H. Bartsch, J. Müller, J. Töpfer, J. Eur. Ceram. Soc. **35**, 3043–3049 (2015)
10. P. Kum-onsa, P. Thongbai, B. Putasaeng, T. Yamwong, S. Maensiri, J. Eur. Ceram. Soc. **35**, 1441–1447 (2015)
11. S. Wu, P. Liu, Y. Lai, W. Guan, Z. Huang, J. Han, Y. Xiang, W. Yi, Y. Zeng, J. Mater. Sci. Mater. Electron. **27**, 10336–10341 (2016)
12. X.W. Wang, P.B. Jia, X.E. Wang, B.H. Zhang, L.Y. Sun, Q.B. Liu, J. Mater. Sci. Mater. Electron. **27**, 12134–12140 (2016)
13. Y. Liu, X. Zhao, C. Zhang, J. Mater. Sci. Mater. Electron. **27**, 11757–11761 (2016)
14. J. Boonlakhorn, P. Kidkhunthod, P. Thongbai, J. Eur. Ceram. Soc. **35**, 3521–3528 (2015)
15. W. Wan, C. Liu, H. Sun, Z. Luo, W.-X. Yuan, H. Wu, T. Qiu, J. Eur. Ceram. Soc. **35**, 3529–3534 (2015)
16. M.A. Ponce, M.A. Ramirez, F. Schipani, E. Joanni, J.P. Tomba, M.S. Castro, J. Eur. Ceram. Soc. **35**, 153–161 (2015)
17. J. Li, P. Liang, J. Yi, X. Chao, Z. Yang, J. Am. Ceram. Soc. **98**, 795–803 (2015)
18. Z. Xu, H. Qiang, J. Mater. Sci. Mater. Electron. **28**, 376–380 (2017)
19. Z. Xu, H. Qiang, Y. Chen, Z. Chen, Mater. Chem. Phys. **191**, 1–5 (2017)
20. Z. Liu, Z. Yang, X. Chao, J. Mater. Sci. Mater. Electron. **27**, 8980–8990 (2016)
21. L. Liu, H. Fan, X. Chen, P. Fang, J. Alloys Compd. **469**, 529–534 (2009)
22. J. Liu, C.-G. Duan, W.-G. Yin, W. Mei, R. Smith, J. Hardy, Phys. Rev. B **70**, 144106 (2004)
23. W. Hao, H. Wu, P. Xu, Y. Shi, S. Yang, M. Wang, L. Sun, E. Cao, Y. Zhang, Ceram. Int. **43**, 3631–3638 (2017)
24. Y. Shi, W. Hao, H. Wu, L. Sun, E. Cao, Y. Zhang, H. Peng, Ceram. Int. **42**, 116–121 (2016)
25. W. Hao, J. Zhang, Y. Tan, M. Zhao, C. Wang, J. Am. Ceram. Soc. **94**, 1067–1072 (2011)
26. T. Adams, D. Sinclair, A. West, Phys. Rev. B **73**, 094124 (2006)
27. S.-Y. Chung, I.-D. Kim, S.-J.L. Kang, Nat. Mater. **3**, 774–778 (2004)
28. L. Ni, X.M. Chen, X.Q. Liu, Mater. Chem. Phys. **124**, 982–986 (2010)
29. L. Ni, X.M. Chen, Solid State Commun. **149**, 379–383 (2009)
30. S.F. Shao, J.L. Zhang, P. Zheng, C.L. Wang, J.C. Li, M.L. Zhao, Appl. Phys. Lett. **91**, 042905 (2007)
31. J. Jumpatam, W. Somphan, B. Putasaeng, N. Chanlek, P. Kidkhunthod, P. Thongbai, S. Maensiri, Mater. Res. Bull. **90**, 8–14 (2017)

32. W. Li, L. Tang, F. Xue, Z. Xin, Z. Luo, G. Du, Ceram. Int. **43**, 6618–6621 (2017)
33. L. Sun, Z. Wang, Y. Shi, E. Cao, Y. Zhang, H. Peng, L. Ju, Ceram. Int. **41**, 13486–13492 (2015)
34. B. Ravel, M. Newville, J. Synchrotron. Radiat. **12**, 537–541 (2005)
35. J. Wu, C.-W. Nan, Y. Lin, Y. Deng, Phys. Rev. Lett. **89**, 217601 (2002)
36. J. Jumpatam, W. Somphan, J. Boonlakhorn, B. Putasaeng, P. Kidkhunthod, P. Thongbai, S. Maensiri. J. Am. Ceram. Soc. **100**, 157–166 (2017)
37. M. Li, G. Cai, D.F. Zhang, W.Y. Wang, W.J. Wang, X.L. Chen, J. Appl. Phys. **104**, 074107 (2008)